

Quasiperiodicity-induced non-Hermitian skin effect from the breakdown of scale-free localization

Kazuma Saito,^{1,2} Ryo Okugawa,¹ Kazuki Yokomizo,³ Takami Tohyama,¹ and Chen-Hsuan Hsu^{2,4}

¹*Department of Applied Physics, Tokyo University of Science, Katsushika, Tokyo 125-8585, Japan*

²*Institute of Physics, Academia Sinica, Taipei 115201, Taiwan*

³*Department of Physics, The University of Tokyo,*

^{7-3-1 Hongo, Bunkyo-ku, Tokyo 113-0033, Japan}

⁴*Physics Division, National Center for Theoretical Sciences, Taipei 106319, Taiwan*

(Dated: February 12, 2026)

Non-reciprocal systems exhibit extreme sensitivity to boundary conditions, typically manifesting as the non-Hermitian skin effect (NHSE) under open boundaries. By bridging the boundaries with a tunable impurity bond, one can access intermediate regimes where scale-free localization (SFL) can emerge. Here, we investigate the competition between such boundary coupling and quasiperiodic disorder in a non-reciprocal lattice. Our analyses reveal a quasiperiodicity-induced breakdown of the SFL regime, which evolves into either the NHSE or an extended regime, depending on boundary conditions. These results uncover the crucial role of quasiperiodicity in non-Hermitian systems.

Introduction. In non-Hermitian systems [1, 2], the non-Hermitian skin effect (NHSE) is one of the most striking phenomena characterized by the exponential localization of a macroscopic number of eigenstates at the system boundaries. This effect is a hallmark of the Hatano-Nelson model [3–5], a paradigm lattice system featuring non-reciprocal hoppings. In this model, complex-valued energies and extended states appear under periodic boundary conditions (PBC), whereas real-valued energies and macroscopic boundary-accumulated states emerge under open boundary conditions (OBC), indicating an extreme sensitivity to boundary conditions. The NHSE under OBC is topologically rooted in the non-trivial point-gap topology of the energy spectrum under PBC, a phenomenon unique to non-Hermitian systems [6–24].

The introduction of quasiperiodicity into non-Hermitian systems gives rise to a richer class of localization phenomena. In the Hermitian setting, the Aubry-Andre-Harper (AAH) model [25, 26] provides a paradigmatic example of a quasiperiodic system exhibiting a global localization transition of all eigenstates upon tuning the quasiperiodic potential strength. In contrast, in the non-Hermitian extension of the AAH model, increasing the quasiperiodic potential strength leads to distinct boundary-dependent transitions: an NHSE-localization transition under OBC and a delocalization-localization transition under PBC [27–43].

To physically control boundary sensitivity, one can introduce a tunable impurity bond connecting the boundaries. Tuning the hopping strength of this single bond allows for a continuous interpolation between the OBC and PBC limits, effectively imposing generalized boundary conditions (GBC) [44–47]. Crucially, this impurity-induced boundary effect modulates the NHSE into a distinct localized regime known as scale-free localization (SFL) [45, 48–59]. In this regime, eigenstates accumulate near the boundaries but possess localization lengths that

scale linearly with the system size, contrasting with the size-independent localization characteristic of the NHSE. Examining this tunable setting disentangles the roles of boundary effects and system sizes.

Beyond their fundamental properties, the strong boundary-condition sensitivity of non-reciprocal systems inherently leads to numerical instability, demanding high computational precision [60, 61]. This instability originates from the non-normality of non-Hermitian Hamiltonians, where left and right eigenstates become highly non-orthogonal. Remarkably, this same non-normality encodes essential information about the underlying wavefunction properties. The condition number, introduced as a quantitative measure of non-normality and numerical instability [11, 60, 62, 63], has recently been identified as an indicator for the NHSE [64]. By employing the condition number, one can thus characterize various regimes under GBC, where conventional topological arguments are not directly applicable.

In this work, we investigate the competition between these two distinct localization mechanisms: the quasiperiodicity-induced bulk localization and non-Hermiticity-induced boundary localization, which can manifest as either the NHSE or the SFL and are tunable via a boundary impurity. We introduce the non-normality ratio as an efficient indicator capable of distinguishing various regimes and constructing the regime diagram across a broad parameter space. In contrast to the naive expectation that increasing quasiperiodicity would smoothly drive the SFL into a localized phase, we report the discovery of a quasiperiodicity-induced NHSE: under SFL regime, increasing the quasiperiodic potential strength drives a breakdown of SFL, which evolves into the NHSE regime before entering the localized phase. Depending on the boundary parameters, an evolution into an extended regime is also observed. The breakdown arises from the quasiperiodicity-induced deformation of the GBC spectrum while preserving the point gap of the

PBC spectrum. These findings provide insights into the interplay among quasiperiodicity, NHSE, and SFL.

Model. We consider a lattice forming a closed loop in which the endpoints are connected by a tunable impurity bond, incorporating non-reciprocal hoppings between nearest-neighbor sites and an onsite quasiperiodic potential, as illustrated in Fig. 1(a),

$$H = -J \sum_{j=1}^{L-1} \left(e^\alpha c_j^\dagger c_{j+1} + e^{-\alpha} c_{j+1}^\dagger c_j \right) + \sum_{j=1}^L \lambda_j c_j^\dagger c_j - \mu J \left(e^\alpha c_L^\dagger c_1 + e^{-\alpha} c_1^\dagger c_L \right). \quad (1)$$

Here, L is the total number of sites, J is the hopping amplitude, and α represents the degree of non-reciprocity. The operators c_j^\dagger (c_j) denote the creation (annihilation) of a fermionic particle at site j . The term $\lambda_j := \lambda \cos(2\pi j/\tau + \phi)$ represents the quasiperiodic potential, where λ denotes the potential strength controlling bulk localization, τ is the wavelength set to the golden ratio, and ϕ is a real phase parameter. In non-reciprocal systems, the bulk localization transition occurs at the critical strength $\lambda_c = 2Je^\alpha$, independent of boundary conditions. Under OBC it marks the NHSE-bulk localization transition [27], while under PBC it corresponds to the delocalization-localization transition [27, 43].

The parameter μ modifies the hopping amplitude across the impurity bond, effectively tuning the boundary condition. Specifically, $\mu = 0$ corresponds to OBC, while $\mu = 1$ recovers PBC, meaning that a value of $\mu \in (0, 1)$ represents GBC [44]. In the absence of quasiperiodicity $\lambda = 0$, the system under GBC exhibits distinct regimes depending on the system size L : the NHSE regime for small L and the SFL regime for large L . These regimes are distinguished based on the scaling of the localization length ξ . Assuming that the wavefunction intensity centered at X is given by

$$|\psi(x)| \propto e^{-|x-X|/\xi}, \quad (2)$$

the system is classified as the NHSE regime if ξ is independent of L , and as the SFL regime if ξ is proportional to L . Further details on the regimes for $\lambda = 0$ are provided in Supplemental Material (SM) [65].

In the numerical calculations, we set J as the overall energy scale and fix the non-reciprocity parameter at $\alpha = 0.5$ (yielding a critical potential strength $\lambda_c \approx 3.3J$). We vary μ and λ over non-negative values to explore the regime diagram. While L is generally varied to extract scaling behavior, a Fibonacci number is chosen for fixed- L plots to minimize the mismatch between the lattice sites and the quasiperiodic modulation. Unless otherwise noted, the quantities are obtained as averages taken over 100 values of ϕ . With the coexisting quasiperiodicity, non-reciprocity, and an impurity bond, we examine the wavefunction profile $|\psi(x)|$ of the right eigenstate

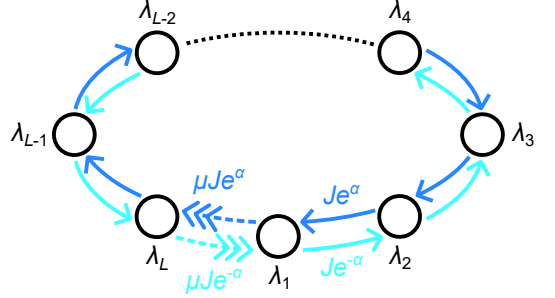


FIG. 1. Schematic illustration of the system, with non-reciprocal hopping strength $Je^{\pm\alpha}$, quasiperiodic onsite potential λ_j , and an impurity bond with hopping strength tunable by μ .

with the second smallest real part, since the smallest one is dominated by the impurity-induced in-gap mode and offers limited information about the quasiperiodicity-induced localization.

Non-normality ratio. The tunable hopping strength across the impurity bond effectively controls the boundary condition, enabling the realization of GBC. In the presence of non-reciprocal hopping, such intermediate boundary conditions give rise to the SFL regime [45, 58], where a macroscopic number of states become exponentially localized near the boundaries, with a localization length proportional to the system size. Since its spectral and localization features merge with those under PBC in the thermodynamic limit, the SFL is essentially a finite-size effect. Nevertheless, it displays behavior distinct from both the NHSE regime and the PBC case. This suggests that the condition number, which measures the non-normality of the Hamiltonian, follows a characteristic scaling law in the SFL regime. We therefore derive this scaling relation in the SFL regime and use it to characterize the system.

The condition number of a system is obtained by computing the singular values $\{s(V)\}$ of a regular matrix V and subsequently finding the product of the spectral norms (the maximum value of the singular values) of V and V^{-1} [60],

$$\kappa(V) := \|V\| \|V^{-1}\| = \frac{s_{\max}(V)}{s_{\min}(V)}, \quad (3)$$

where the columns of V are given by the right eigenvectors $|E_n^a\rangle$ of the n -th energy level with degeneracy index a . Since the condition number depends on the choice of basis for degenerate eigenvectors, we denote it as $\kappa(V)$ to explicitly indicate its dependence on V . For the calculation of the condition number, we choose a basis such that the right eigenvectors are orthonormal:

$$\langle E_n^a | E_n^b \rangle = \delta_{ab}, \quad (4)$$

where E_n^a denotes the eigenvectors. This leads to a well-behaved and unique condition number, which equals

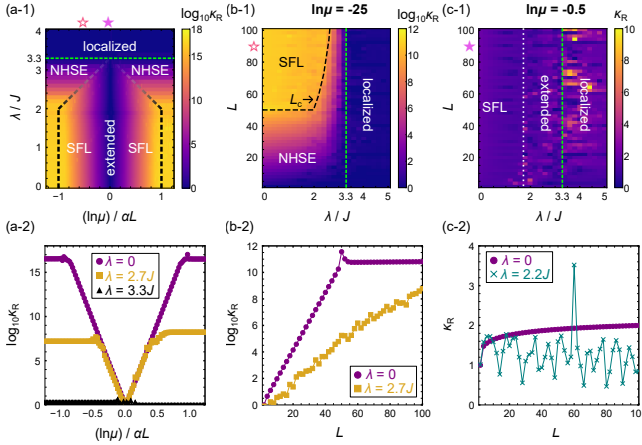


FIG. 2. (a-1) Non-normality ratio-based regime diagram on the $(\ln \mu, \lambda)$ plane for $L = 89$ and $\phi = 0$. The black-gray dashed line represents the NHSE-SFL boundary. Specific values on the $\ln \mu / (\alpha L)$ axis are indicated by an open star (≈ -0.56) and a solid star (≈ -0.01). The corresponding parameters for $L = 89$ in (b-1) and (c-1) are indicated by the same symbols. (a-2) μ -dependence of $\log_{10} \kappa_R$ corresponding to cuts in (a-1). (b-1, c-1) Regime diagrams on the (λ, L) plane for (b-1) $\ln \mu = -25$ and (c-1) $\ln \mu = -0.5$. The dashed curves correspond to the boundary shown in (a-1). (b-2, c-2) Scaling behavior of κ_R for the parameters used in (b-1) and (c-1), respectively.

to unity when the Hamiltonian is normal. Moreover, its value can be bounded within a range not exceeding \sqrt{L} times the theoretically minimal condition number, thereby preventing overestimation [64]. For the condition number calculated in this basis, we omit the variable V from the notation. As discussed below, the regimes can be distinguished by examining the scaling law of the condition number, $\kappa = O(e^{L/\xi})$, under the assumption that all wave functions are exponentially localized at the boundary. The details of the derivation are provided in the SM [65].

To eliminate the bulk contribution, which is independent of boundary conditions, we define *non-normality ratio* as

$$\kappa_R(\mu) := \frac{\kappa_{\text{GBC}}(\mu)}{\kappa_{\text{PBC}}}, \quad (5)$$

where κ_{GBC} is the condition number under GBC at a given μ , and κ_{PBC} is that under PBC ($\mu = 1$). This quantity provides an efficient means to distinguish among the NHSE, NFL, and other regimes, using $\kappa = O(e^{L/\xi})$. For the NHSE, where the localization length ξ is constant, the condition number grows exponentially with system size. In the NFL, κ_R is of order $e^{L/\xi}$ with ξ linearly scaling with L . In contrast, for bulk states in the extended, critical, or localized phases, the contribution from the boundaries is absent, and κ_R always remains of order unity as L varies.

Regime diagram for general μ and λ . Figure 2(a-1) dis-

plays the regime diagram in the $(\ln \mu, \lambda)$ plane. The horizontal axis is normalized by αL . Our numerical verification confirms that the diagram is obtained independently of L for sufficiently large system sizes. Here, $\ln \mu = 0$ corresponds to the PBC limit, where the system undergoes a sharp transition from the extended to the localized phase at λ_c . The green dashed line indicates this critical λ_c value, representing the bulk localization transition that persists for any μ , as inferred from the entanglement spectrum; see SM [65] for details.

Interesting features emerge in the $\lambda < \lambda_c$ regime with $0 < |\ln \mu| < \alpha L$. As shown in Fig. 2(a-2), for each $\lambda < \lambda_c$, the dependence of $\log_{10} \kappa_R$ on $|\ln \mu|$ is divided into two distinct regimes: a linearly increasing region and a plateau where the value remains constant. The plateau region corresponds to an effective OBC regime where the influence of impurity bonds either vanishes or becomes dominant; here, the system exhibits the characteristics of the NHSE. The linear region represents an intermediate regime between the NHSE and the extended phase, which can be identified as the NFL regime. Notably, the value of μ at which this transition occurs depends on λ . We indicate this regime boundary by a black-gray dashed line in Fig. 2(a-1). As λ approaches λ_c , the system approaches the bulk localized phase, causing κ_R to tend toward $O(1)$. Consequently, the NFL region is compressed by the plateau, making regime identification difficult. The gradient of the boundary line reflects this behavior. We refer to this transition as a crossover between the NFL regime governed by intermediate boundary conditions and the NHSE regime under effective OBC.

In Figs. 2(b) and 2(c), we present the non-normality ratio in a broad parameter regime. Here we focus on $\ln \mu = -25$ and -0.5 ; the corresponding results for $\ln \mu > 0$ and the regime diagram for general μ are shown in SM [65]. Figure 2(b-1) presents the results in the (λ, L) plane under GBC with $\ln \mu = -25$, where an NHSE-NFL crossover occurs at a λ -dependent critical length L_c (black curve) within the regime $\lambda < \lambda_c$. One can see that the critical length follows roughly the relation $L_c \propto 1/|\lambda - \lambda_c|$ at $\lambda > 2J$, consistent with the crossover line shown in Fig. 2(a-1). At $\lambda = 0$, the critical length is $L_c = 50$, consistent with the analytical estimate presented in SM [65] as well as in previous studies [45, 53]. For $\lambda = 2.7J$, L_c is estimated to be 109. Indeed, the regime at $L = 89$ shown in Fig. 2 exhibits the properties of the NHSE. To examine the scaling behavior more closely, we plot the length dependence in Fig. 2(b-2). In the NHSE regime, κ_R increases exponentially with L , until it reaches the order of 10^{10} . For $L > L_c$, the scaling transits into an approximately logarithmic behavior, as expected for the NFL regime.

Figure 2(c-1) shows the region near the PBC limit with $\ln \mu = -0.5$. Here, the system exhibits the NFL regime for small λ . At $\lambda = 0$, κ_R increases logarithmically with L [see Fig. 2(c-2)]. For increasing potential strength but

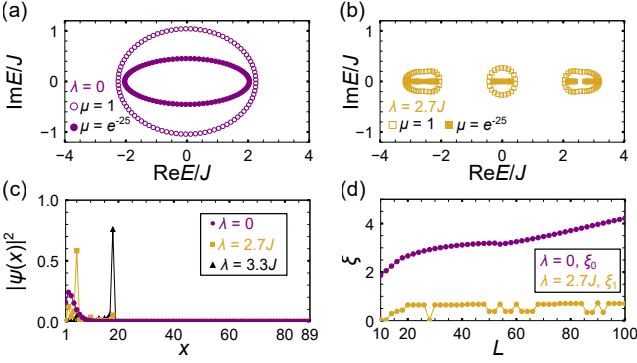


FIG. 3. Characteristics of various regimes for $\phi = 0$ and representative λ and μ values. (a,b) Energy spectra for $L = 89$. The closed (open) symbols represent the spectra for $\ln \mu = -25$ ($\mu = 1$). (c) Spatial distributions of the density $|\psi(x)|^2$ for $L = 89$ and $\ln \mu = -25$. (d) Localization lengths, ξ_0 (for $\lambda = 0$) and ξ_1 (for $\lambda = 2.7J$), for $\ln \mu = -25$.

still $\lambda < 1.7J$, κ_R shows increasing behavior, with the growth rate gradually suppressed. This increasing trend vanishes at $\lambda \approx 1.7J$, which, according to Eq. (5), implies that the localization properties of the wavefunction begin to coincide with those under PBC. Therefore, based on the phase diagram for PBC, we identify the region $1.7J < \lambda < \lambda_c$ as an extended regime. Indeed, at $\lambda = 2.2J$, we observe that κ_R does not increase with L [see Fig. 2(c-2)]. As a remark, consistent with Fig. 2(a-1), the results for $\ln \mu = -0.5$ and $\ln \mu = 0.5$ are similar (though not identical) [45]; see SM [65] for the latter case.

Quasiperiodicity-induced NHSE. To examine the NHSE regime induced by strong λ , we analyze the energy spectrum, the spatial distribution of eigenstates, and the localization length for representative μ and λ values, as displayed in Fig. 3. We first examine the PBC ($\ln \mu = 0$) and GBC ($\ln \mu = -25$) energy spectra for a fixed L . For $\lambda = 0$, as shown in Fig. 3(a), the GBC spectrum remains complex and lies inside the PBC one as typical of the SFL regime [45, 48–53, 56–59]. In stark contrast, for $\lambda = 2.7J$, the GBC spectrum completely collapses onto the real axis within the complex PBC loop, as shown in Fig. 3(b). This spectral reality provides unambiguous evidence of the genuine emergence of the NHSE regime, marking a breakdown of the SFL regime observed in the absence of quasiperiodicity.

Figure 3(c) shows the spatial distribution of the density $|\psi(x)|^2$. We identify distinct peak positions characteristic of the SFL ($\lambda = 0$), NHSE ($\lambda = 2.7J$), and localized ($\lambda = 3.3J$) regimes for a fixed L , denoted as X_0 , X_1 , and X_2 , respectively. In the intermediate range $2J \lesssim \lambda \lesssim 3.3J$, peaks at these positions coexist; as λ increases the intensity at X_0 continuously diminishes while that at X_1 becomes dominant, followed by the gradual emergence of the bulk peak at X_2 . This continuous transfer of spectral weight between spatially distinct

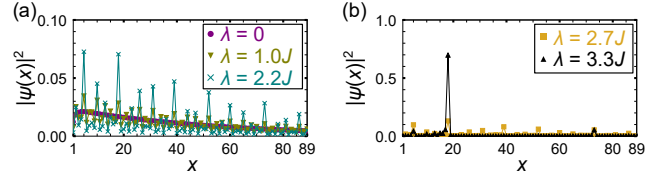


FIG. 4. Spatial distributions of the density $|\psi(x)|^2$ for $L = 89$, $\ln \mu = -0.5$ and $\phi = 0$ (a) for SFL and extended states and (b) for extended and localized states.

modes justifies identifying the SFL-NHSE transition as a crossover. To quantitatively analyze this behavior and extract the corresponding localization lengths, we model the wavefunction profile of (right) eigenstate with the second-smallest real part of its eigenvalue using a multi-peak ansatz with the fixed peak positions $X_{0,1,2}$:

$$|\psi(x)| = A_0 e^{-|x-X_0|/\xi_0} + A_1 e^{-|x-X_1|/\xi_1} + A_2 e^{-|x-X_2|/\xi_2}, \quad (6)$$

where $A_{0,1,2}$ and $\xi_{0,1,2}$ are the fitting parameters representing the amplitudes and localization lengths of the respective components.

Figure 3(d) shows the scaling of the localization lengths $\xi_{0,1}$ obtained by fitting the wavefunction to Eq. (6). For $\lambda = 0$, only the peak at X_0 exists. Except for very small systems, the ξ_0 value goes from approximately constant to scaling linearly with L beyond a certain system size, indicating a crossover from the NHSE regime to the SFL regime at the critical length $L_c = 50$ [45, 65]. In contrast, for $\lambda = 2.7J$, peaks at X_0 , X_1 , and X_2 are present, but the peak at X_1 is dominant. The ξ_1 value is nearly independent of L , exhibiting NHSE behavior, even beyond $L = 50$. We find an NHSE regime appearing between $\lambda = 2J$ (the critical value in the Hermitian limit, $\alpha = 0$) and the corresponding critical value, $\lambda_c \approx 3.3J$, of the present system, as shown in Fig. 2(a-1). By contrast, in systems with purely unidirectional hopping [58], the transition between the SFL regime and the localized phase occurs exactly at $\lambda = 2J$, and this quasiperiodicity-induced NHSE regime is absent in the large- L limit, as it shrinks to a negligible range.

Due to the effect of quasiperiodicity, the spectral loops close as the system approaches the bulk localization transition. Since the GBC spectrum lies inside the PBC spectrum, it collapses into line segments at a smaller λ value than the PBC spectrum. Consequently, an NHSE regime emerges between the SFL regime and the localized phase. From a real-space perspective, the effective OBC is realized because the quasiperiodic potential suppresses the hopping across the impurity bond prior to the hoppings in the bulk; further details are provided in SM [65]. In the thermodynamic limit, the emerging NHSE region collapses to the critical point λ_c , where the SFL regime evolves into the extended regime as $\xi \rightarrow \infty$. Consequently, for $L \rightarrow \infty$, the system exhibits a delocalization-

localization transition analogous to that under PBC.

Quasiperiodicity-assisted delocalization. Interestingly, our results suggest that when the system is under GBC but remains close to the PBC limit, increasing λ drives a crossover from the SFL regime to an extended regime. Below, we analyze this delocalization in more detail by examining the wavefunction profiles in Fig. 4.

As illustrated in Fig. 4(a), the SFL-localized profile gradually evolves into an extended wave-like form as λ increases, and eventually undergoes a delocalization-localization transition similar to that under PBC [see Fig. 4(b)]. In this μ regime, the PBC ($\mu = 0$) and GBC ($\mu = e^{-0.5}$) spectra are nearly identical for $\lambda \geq 0$; increasing λ suppresses the difference even further. As a result, the system undergoes a crossover from the SFL regime to an extended regime. Because μ is close to unity, the boundary conditions effectively approach PBC, favoring the extended regime. This behavior contrasts with the large $|\ln \mu|$ case, where the intermediate regime is the NHSE. Such quasiperiodicity-assisted delocalization underscores another nontrivial interplay between quasiperiodicity and the SFL regime.

Discussion. Generally, increasing the quasiperiodic potential is expected to suppress the NHSE or extended states, driving the system toward bulk localization. Contrary to this conventional scenario, we find that when the system is in the SFL regime, quasiperiodicity destroys this state, inducing an extended regime near the PBC limit and the NHSE regime far from it, before eventually entering the boundary-independent localized phase. We attribute the origin of this behavior to the distinct responses of the PBC spectrum and the GBC spectrum to the quasiperiodic potential.

In non-reciprocal systems, characterization of different regimes is typically based on the spectral winding number [7, 11, 66], a topological invariant defined only under PBC and thus inapplicable under GBC. Alternative approaches employ boundary-condition-insensitive quantities, such as the entanglement entropy [39, 40, 53, 67], but their numerical evaluation requires high precision and is computationally demanding; for completeness, we present the corresponding entanglement-based regime diagram of our system in SM [65]. We further note that the accuracy of the entanglement entropy itself depends on the condition number [63]. Therefore, characterizing regimes through the introduced non-normality ratio, quantified directly by the condition number under GBC, offers the most direct and efficient approach.

Non-reciprocal systems with non-Hermitian impurities and random disorder have already been experimentally realized in electrical circuits [47], where the SFL has also been observed. Replacing random disorder with quasiperiodic modulation offers a natural route toward realizing the present model in experiments. Such a setup would enable direct observation of the predicted quasiperiodicity-assisted NHSE and delocalization, pro-

viding a versatile platform to explore the interplay among quasiperiodicity, non-Hermiticity, and boundary conditions.

Acknowledgments. We thank N. Okuma, M. Oshikawa, and K. Totsuka for interesting discussions. This work was financially supported by the National Science and Technology Council (NSTC), Taiwan (Grant No. NSTC-114-2112-M-001-057), Academia Sinica (AS), Taiwan (Grant No. AS-iMATE-114-12), JST SPRING, Japan (Grant No. JP-MJSP2151), and JSPS KAKENHI, Japan (Grant No. 23K13027, No. JP23K13033, No. JP24K00586, and No. JP25H01248).

DATA AVAILABILITY

The data that support the findings of this study are available at Zenodo [68].

- [1] C. M. Bender, *Rep. Prog. Phys.* **70**, 947 (2007).
- [2] N. Okuma and M. Sato, *Ann. Rev. Condens. Matter Phys.* **14**, 83 (2023).
- [3] N. Hatano and D. R. Nelson, *Phys. Rev. Lett.* **77**, 570 (1996).
- [4] N. Hatano and D. R. Nelson, *Phys. Rev. B* **56**, 8651 (1997).
- [5] N. Hatano and D. R. Nelson, *Phys. Rev. B* **58**, 8384 (1998).
- [6] S. Yao and Z. Wang, *Phys. Rev. Lett.* **121**, 086803 (2018).
- [7] Z. Gong, Y. Ashida, K. Kawabata, K. Takasan, S. Higashikawa, and M. Ueda, *Phys. Rev. X* **8**, 031079 (2018).
- [8] C. H. Lee, L. Li, and J. Gong, *Phys. Rev. Lett.* **123**, 016805 (2019).
- [9] K. Kawabata, K. Shiozaki, M. Ueda, and M. Sato, *Phys. Rev. X* **9**, 041015 (2019).
- [10] D. S. Borgnia, A. J. Kruchkov, and R.-J. Slager, *Phys. Rev. Lett.* **124**, 056802 (2020).
- [11] N. Okuma, K. Kawabata, K. Shiozaki, and M. Sato, *Phys. Rev. Lett.* **124**, 086801 (2020).
- [12] T. Yoshida, T. Mizoguchi, and Y. Hatsugai, *Phys. Rev. Res.* **2**, 022062 (2020).
- [13] K. Zhang, Z. Yang, and C. Fang, *Phys. Rev. Lett.* **125**, 126402 (2020).
- [14] K. Kawabata, M. Sato, and K. Shiozaki, *Phys. Rev. B* **102**, 205118 (2020).
- [15] R. Okugawa, R. Takahashi, and K. Yokomizo, *Phys. Rev. B* **102**, 241202 (2020).
- [16] Y. Fu, J. Hu, and S. Wan, *Phys. Rev. B* **103**, 045420 (2021).
- [17] S. Longhi, *Phys. Rev. B* **103**, 054203 (2021).
- [18] R. Okugawa, R. Takahashi, and K. Yokomizo, *Phys. Rev. B* **103**, 205205 (2021).
- [19] F. Schindler, K. Gu, B. Lian, and K. Kawabata, *PRX Quantum* **4**, 030315 (2023).
- [20] S. Hamanaka, K. Yamamoto, and T. Yoshida, *Phys. Rev. B* **108**, 155114 (2023).
- [21] D. Nakamura, K. Inaka, N. Okuma, and M. Sato, *Phys. Rev. Lett.* **131**, 256602 (2023).

[22] X.-R. Ma, K. Cao, X.-R. Wang, Z. Wei, Q. Du, and S.-P. Kou, *Phys. Rev. Res.* **6**, 013213 (2024).

[23] T. Yoshida, S.-B. Zhang, T. Neupert, and N. Kawakami, *Phys. Rev. Lett.* **133**, 076502 (2024).

[24] S. Hamanaka, T. Yoshida, and K. Kawabata, *Phys. Rev. Lett.* **133**, 266604 (2024).

[25] P. G. Harper, *Proc. Phys. Soc. Sect. A* **68**, 874 (1955).

[26] S. Aubry and G. André, *Ann. Isr. Phys. Soc.* **3**, 133 (1980).

[27] H. Jiang, L.-J. Lang, C. Yang, S.-L. Zhu, and S. Chen, *Phys. Rev. B* **100**, 054301 (2019).

[28] S. Longhi, *Phys. Rev. Lett.* **122**, 237601 (2019).

[29] S. Longhi, *Phys. Rev. B* **100**, 125157 (2019).

[30] Y. Liu, X.-P. Jiang, J. Cao, and S. Chen, *Phys. Rev. B* **101**, 174205 (2020).

[31] Q.-B. Zeng and Y. Xu, *Phys. Rev. Res.* **2**, 033052 (2020).

[32] T. Liu, H. Guo, Y. Pu, and S. Longhi, *Phys. Rev. B* **102**, 024205 (2020).

[33] Y. Liu, Y. Wang, Z. Zheng, and S. Chen, *Phys. Rev. B* **103**, 134208 (2021).

[34] S. Longhi, *Phys. Rev. B* **104**, 125109 (2021).

[35] L.-J. Zhai, G.-Y. Huang, and S. Yin, *Phys. Rev. B* **106**, 014204 (2022).

[36] W. Chen, S. Cheng, J. Lin, R. Asgari, and G. Xianlong, *Phys. Rev. B* **106**, 144208 (2022).

[37] L.-J. Zhai, L.-L. Hou, Q. Gao, and H.-Y. Wang, *Front. Phys.* **10**, 1098551 (2022).

[38] A. P. Acharya and S. Datta, *Phys. Rev. B* **109**, 024203 (2024).

[39] L. Zhou, *Phys. Rev. B* **109**, 024204 (2024).

[40] S.-Z. Li, X.-J. Yu, and Z. Li, *Phys. Rev. B* **109**, 024306 (2024).

[41] S. R. Padhi, A. Padhan, S. Banerjee, and T. Mishra, *Phys. Rev. B* **110**, 174203 (2024).

[42] X. Tong, Y. Zhang, B. Li, and X. Yang, *Phys. Rev. B* **111**, 214202 (2025).

[43] Y.-P. Wang, C.-K. Chang, R. Okugawa, and C.-H. Hsu, *Phys. Rev. Res.* **7**, 043353 (2025).

[44] R. Koch and J. C. Budich, *Eur. Phys. J. D* **74**, 70 (2020).

[45] L. Li, C. H. Lee, and J. Gong, *Commun. Phys.* **4**, 42 (2021).

[46] C.-X. Guo, C.-H. Liu, X.-M. Zhao, Y. Liu, and S. Chen, *Phys. Rev. Lett.* **127**, 116801 (2021).

[47] H. Wang, J. Liu, T. Liu, and W. Ju, *Front. Phys.* **20**, 014203 (2025).

[48] L. Li, C. H. Lee, S. Mu, and J. Gong, *Nat. Commun.* **11**, 5491 (2020).

[49] Y. Liu, Y. Zeng, L. Li, and S. Chen, *Phys. Rev. B* **104**, 085401 (2021).

[50] K. Yokomizo and S. Murakami, *Phys. Rev. B* **104**, 165117 (2021).

[51] P. Molignini, O. Arandes, and E. J. Bergholtz, *Phys. Rev. Res.* **5**, 033058 (2023).

[52] B. Li, H.-R. Wang, F. Song, and Z. Wang, *Phys. Rev. B* **108**, L161409 (2023).

[53] Y.-C. Wang, H. H. Jen, and J.-S. You, *Phys. Rev. B* **108**, 085418 (2023).

[54] Z. Jiang, R. Okamoto, and H. Obuse, *Phys. Rev. B* **109**, 235408 (2024).

[55] T. Sawada, K. Sone, R. Hamazaki, Y. Ashida, and T. Sagawa, *Phys. Rev. Lett.* **132**, 046602 (2024).

[56] G.-J. Liu, J.-M. Zhang, S.-Z. Li, and Z. Li, *Phys. Rev. A* **110**, 012222 (2024).

[57] D. Peng, S. Cheng, and G. Xianlong, *Phys. Rev. B* **111**, 094204 (2025).

[58] Y. Zhang, L. Su, and S. Chen, *Phys. Rev. B* **111**, L140201 (2025).

[59] Y. Shigedomi and T. Yoshida, *Phys. Rev. B* **113**, 035121 (2026).

[60] L. N. Trefethen and M. Embree, *Spectra and Pseudospectra* (Princeton University Press, Princeton, 2005).

[61] F. Lucas Metz, I. Neri, and T. Rogers, *J. Phys. A: Math. Theor.* **52**, 434003 (2019).

[62] Y. Ashida, Z. Gong, and M. Ueda, *Adv. Phys.* **69**, 249 (2020).

[63] X. Feng, S. Liu, S.-X. Zhang, and S. Chen, *Phys. Rev. B* **111**, 224310 (2025).

[64] Y. O. Nakai, N. Okuma, D. Nakamura, K. Shimomura, and M. Sato, *Phys. Rev. B* **109**, 144203 (2024).

[65] See Supplemental Material for details on the analysis of the model in the absence of quasiperiodicity, the derivation of the scaling law of condition number, the regime diagram characterized by entanglement entropy, the regime diagram in the strong impurity regime, and disconnection of an impurity bond via quasiperiodicity.

[66] J. Claes and T. L. Hughes, *Phys. Rev. B* **103**, L140201 (2021).

[67] K. Kawabata, T. Numasawa, and S. Ryu, *Phys. Rev. X* **13**, 021007 (2023).

[68] K. Saito, *Data for research on regimes in a non-Hermitian quasiperiodic system with an impurity bond* (2026).

Supplemental Materials for “Quasiperiodicity-induced non-Hermitian skin effect from the breakdown of scale-free localization”

Kazuma Saito,^{1,2} Ryo Okugawa,¹ Kazuki Yokomizo,³ Takami Tohyama,¹ and Chen-Hsuan Hsu^{2,4}

¹*Department of Applied Physics, Tokyo University of Science, Katsushika, Tokyo 125-8585, Japan*

²*Institute of Physics, Academia Sinica, Taipei 11529, Taiwan*

³*Department of Physics, The University of Tokyo, 7-3-1 Hongo, Bunkyo-ku, Tokyo 113-0033, Japan*

⁴*Physics Division, National Center for Theoretical Sciences, Taipei 106319, Taiwan*

I. ANALYSIS OF THE SYSTEM IN THE ABSENCE OF THE QUASIPERIODIC POTENTIAL

In this section, we review the basic properties of our system when the quasiperiodic potential is absent $\lambda \rightarrow 0$. By applying the imaginary gauge transformation

$$c_j \rightarrow e^{-\alpha j} c_j, \quad c_j^\dagger \rightarrow e^{\alpha j} c_j^\dagger, \quad (\text{S1})$$

the Hamiltonian (1) without the quasiperiodic potential can be rewritten as

$$H = -J \sum_{j=1}^{L-1} (c_j^\dagger c_{j+1} + c_{j+1}^\dagger c_j) - \mu J (e^{\alpha L} c_L^\dagger c_1 + e^{-\alpha L} c_1^\dagger c_L). \quad (\text{S2})$$

The relation between the hopping amplitude across the impurity bond and that within the bulk determines whether the energy eigenvalues under the generalized boundary conditions (GBC) are real or complex [1, 2].

In particular, in the regime where μ is sufficiently small, the hopping across the impurity bond can be approximated to be unidirectional and the problem can be treated analytically. For this purpose, we consider this approximated model,

$$H' = -J \sum_{j=1}^{L-1} (c_j^\dagger c_{j+1} + c_{j+1}^\dagger c_j) - \mu J e^{\alpha L} c_L^\dagger c_1, \quad (\text{S3})$$

and determine its eigenenergies. Assuming the eigenstate $\psi_n = C_1 z_1^n + C_2 z_2^n$, where C_1 and C_2 are constants, z_1 and z_2 are the roots of the eigenvalue equation $E = J(z + z^{-1})$ satisfying $z_1 z_2 = 1$, and imposing the boundary conditions $\psi_0 = 0$ and $\psi_{L+1} = \mu e^{\alpha L}$, we set $z_1 = e^{i\theta}$. From the eigenvalue equation, we obtain

$$E = 2J \cos \theta, \quad \text{where} \quad \sin[(L+1)\theta] = \mu e^{\alpha L} \sin \theta. \quad (\text{S4})$$

The eigenenergy becomes complex when $\mu e^{\alpha L} \geq 1$, from which we can estimate that the non-Hermitian skin effect (NHSE) is broken and the scale free localization (SFL) occurs at $\mu = e^{-\alpha L}$ when increasing μ from zero.

Next, by further increasing μ , we determine the value of μ at which the approximation (S3) does not apply. In this regime, only the hopping across the impurity dominates, and the eigenenergies are expected to become real. This corresponds to the condition, $\mu e^{-\alpha L} > 1$, from which we can estimate that the NHSE recovers at $\mu = e^{-\alpha(L+1)}$.

In the weak ($\mu \ll 1$) and strong ($\mu \gg e^\alpha$) impurity limits, the eigenstates for sufficiently large L can be obtained analytically, and in both cases, they are found to be SFL states [3].

The regime diagram of this model has been obtained in Ref. [3], and here we present it in Fig. S1(a) for illustration. The above estimation of the SFL-NHSE critical length is consistent with the previous numerical analysis. In the intermediate region of μ ($e^{-2\alpha} < \mu < e^{2\alpha}$), the system exhibits an SFL regime localized near $j = 1$, similar to the NHSE regime, for $\mu < 1$, and a reversed SFL (rSFL) regime localized near the opposite edge at $j = L$ for $\mu > 1$. At $\mu = e^{2\alpha}$, an extended regime, referred to as the quasi-periodic boundary conditions (quasi-PBC), emerges between the sharp transition between the sharp transition from the rSFL to the SFL regime. Figure S1(b) shows the representative density profiles in each of the regimes.

In the main text, we consider the case $\lambda \neq 0$. When quasiperiodicity, non-reciprocity, and GBC coexist, the eigenstate with the smallest real part is typically dominated by an impurity-induced in-gap mode. To gain insight into the localization properties, we therefore examine the wavefunction profile of the right eigenstate with the second smallest real part. In the complex spectrum, this state lies at the band edge and, in our model, always possesses a real eigenvalue.

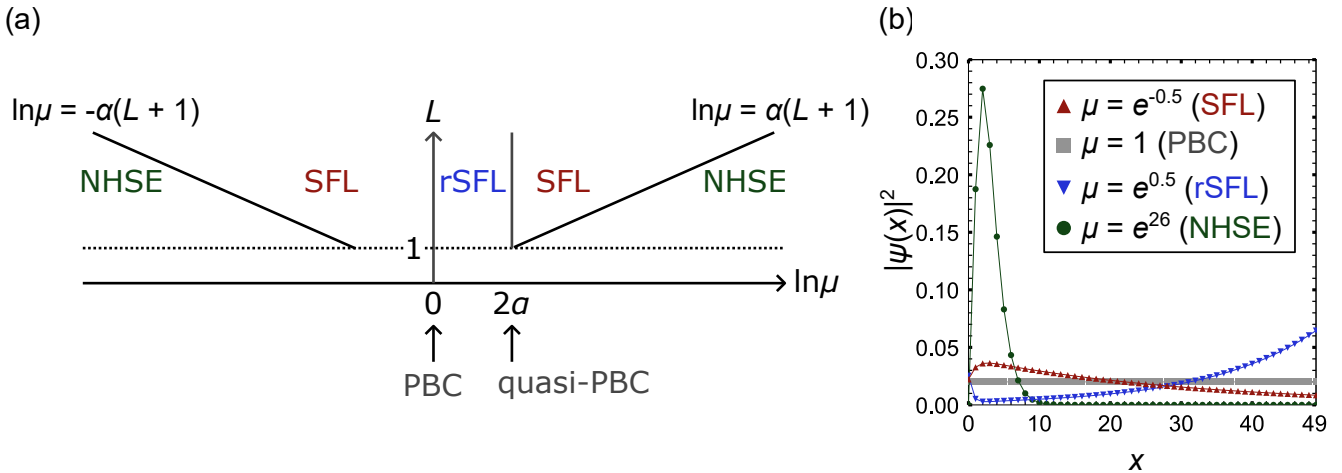


FIG. S1. (a) Regime diagram of the model (S2) for $\lambda = 0$ in the $(\ln \mu, L)$ plane. (b) Spatial distributions of the density in various regimes for $\alpha = 0.5$ and $L = 50$.

II. THE CONDITION NUMBER AND REGIMES

Here, we derive scaling laws of the condition number in each regime. From the inequality between the spectral norm and the Frobenius norm of an $L \times L$ matrix A [4],

$$\sqrt{\text{tr}(A^\dagger A)/L} \leq \|A\| \leq \sqrt{\text{tr}(A^\dagger A)}, \quad (\text{S5})$$

the condition number $\kappa(V)$ defined in Eq. (3) satisfies

$$\begin{aligned} & \sqrt{\text{tr}(V^\dagger V)/L} \sqrt{\text{tr}\{(V^{-1})^\dagger V^{-1}\}/L} \leq \kappa(V) \leq \sqrt{\text{tr}(A^\dagger A)} \sqrt{\text{tr}\{(V^{-1})^\dagger V^{-1}\}} \\ & \Rightarrow \sqrt{\frac{1}{L} \sum_{n,a} \langle\langle E_n^a | E_n^a \rangle\rangle} \leq \kappa(V) \leq \sqrt{L \sum_{n,a} \langle\langle E_n^a | E_n^a \rangle\rangle}, \end{aligned} \quad (\text{S6})$$

with the left eigenvector $|E_n^a\rangle\rangle$. To obtain the second line, we used the normalization condition of the basis defined in Eq. (4).

Assuming that all the wavefunctions $\langle x | E_n^a \rangle$ take the form as in Eq. (2) with the same localization center $X = 0$ and the same localization length ξ , we can derive upper and lower bounds for the condition number. From Eq. (4), the normalization constant of the right wavefunction is estimated to be approximately unity. Additionally, using the biorthogonality condition for the left and right eigenstates,

$$\langle\langle E_n^a | E_m^b \rangle\rangle = \delta_{nm} \delta_{ab}, \quad (\text{S7})$$

the normalization constant of the left wavefunction is estimated as $1/\sqrt{L}$. Consequently, the inner product of the left eigenvectors is given by

$$\langle\langle E_n^a | E_n^a \rangle\rangle \approx e^{2L/\xi}/L. \quad (\text{S8})$$

Combining these results, we obtain

$$\sqrt{\sum_{n,a} \langle\langle E_n^a | E_n^a \rangle\rangle} \approx e^{L/\xi} \quad (\text{S9})$$

If the system is in the NHSE regime where ξ is independent of L , κ follows an exponential law with respect to L . Conversely, in the SFL regime where ξ is proportional to L , κ does not exhibit an exponential scaling law. Note that even in the SFL case, κ is of the order of $e^{L/\xi}$, which allows us to distinguish it from bulk states that are strictly $O(1)$.

III. CHARACTERIZING REGIMES VIA THE ENTANGLEMENT ENTROPY

In this section, we discuss the entanglement entropy (EE), which is defined for a given real-space many-body state and serves as a measure of how inhomogeneously that state is distributed. When using EE as a quantity to characterize the system, it is appropriate to consider its value in the steady state reached after long-time evolution.

To proceed, we consider a system of N free fermions, and denote the state at time t by $|\Psi_t\rangle$. The state $|\Psi_t\rangle$ is represented as a collection of N mutually orthogonal single-particle state vectors. For the initial state, we take a half-filled and evenly distributed state in the real-space representation, where particles occupy every other site:

$$|\Psi_0\rangle = \prod_{j=1}^{\lfloor L/2 \rfloor} c_{2j-1}^\dagger |0\rangle, \quad (\text{S10})$$

with the vacuum state $|0\rangle$. By applying the time-evolution operator e^{iHt} , we obtain the time-evolved state.

Since this is a fermionic system, the single-particle states within $|\Psi_t\rangle$ must remain orthogonal. To preserve this orthogonality, we follow the procedure discussed in Ref. [5] to perform the time evolution. Specifically, we express the state at time t as

$$|\Psi_t\rangle = \prod_{n=1}^N \left\{ \sum_{j=1}^L U_{jn}(t) c_j^\dagger \right\} |0\rangle, \quad (\text{S11})$$

where U is an $L \times N$ matrix. For example, at $t = 0$, we have $U_{jn}(0) = \delta_{j,2n-1}$. To evolve this state by a time step Δt , we compute $e^{iH\Delta t}U$, and then perform a QR decomposition,

$$e^{iH\Delta t}U = QR, \quad (\text{S12})$$

from which we obtain the new orthonormalized state $U(t + \Delta t) = Q$.

Since $U(t)$ represents the N -particle state at time t , the correlation matrix is given by

$$C(t) = [U(t)U^\dagger(t)]^T, \quad (\text{S13})$$

which yields the correlation function $C_{jk}(t) = \langle \Psi_t | c_j^\dagger c_k | \Psi_t \rangle$. The superscript T represents the transposition. We then restrict the correlation matrix to an $l \times l$ sub-block, corresponding to partitioning the system into subsystems of size l and $L-l$. By diagonalizing this block, we obtain the eigenvalues $\zeta_j(t)$, from which the EE at time t is calculated as

$$S_l(t) = - \sum_{j=1}^l [\zeta_j(t) \ln \zeta_j(t) + \{1 - \zeta_j(t)\} \ln \{1 - \zeta_j(t)\}]. \quad (\text{S14})$$

In our calculations, we set $\Delta t = 1$ and $l = L/2$. The steady-state value of $S_{L/2}$ was obtained by averaging its values over the interval $t = 1000$ to 2000 to ensure that a steady state is reached.

In systems with non-reciprocal hopping, the entanglement entropy $S_{L/2}$ follows a logarithmic law for extended or SFL regimes, an area law for localized or NHSE regimes, and a volume law for critical states, depending on the localization properties of the particles [2, 6, 7].

We summarize our results in Fig. S2. Taking several μ values as representatives, we observe that the crossover in the scaling behavior of the EE in each μ region coincides with the change in the scaling of the non-normality ratio presented in Fig. 2 in the main text and Fig. S3 (see below). At the bulk localization transition point $\lambda = \lambda_c$, the EE follows the volume law, while in the localized phase for $\lambda > \lambda_c$, it obeys the area law. For $\lambda < \lambda_c$, Figs. S2(a) show that EE follows the area law for small L due to the NHSE and the logarithmic law for large L due to the SFL, with the corresponding crossover length increasing with λ . In Figs. S2(b), the EE follows a logarithmic law, consistent with the SFL [2] or the extended regime [6, 7].

IV. REGIME DIAGRAM IN THE STRONG IMPURITY REGIONS

In this section, we consider the case where the hopping across the impurity is stronger than other bonds and present Fig. S3. For $\ln \mu = 0.5$, which is close to the PBC limit, a crossover is found from the rSFL regime, where the non-normality ratio follows a logarithmic scaling law, to the extended regime, where it is constant as shown in Fig. S3(a).

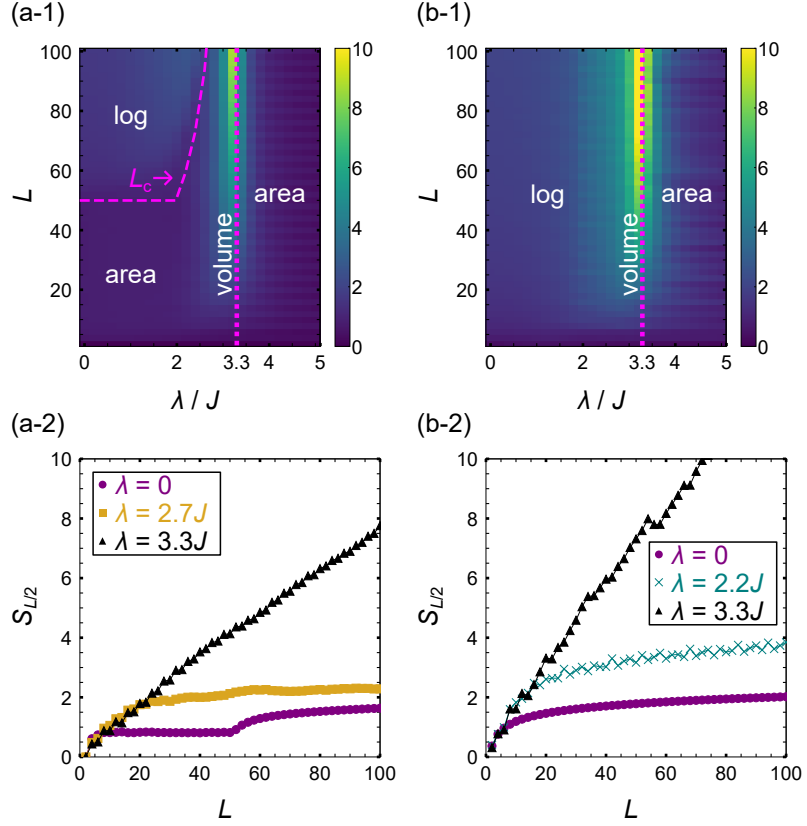


FIG. S2. (a-1,b-1) Entanglement-based regime diagrams under GBC. The color bar represents $S_{L/2}$. (a-2,b-2) Scaling behavior of the EE. The corresponding impurity strengths correspond to (a) $\ln \mu = -25$, (b) $\ln \mu = -0.5$.

For large impurity strength ($\ln \mu = 25$), a regime diagram in Fig. S3(c) similar to Fig. 2(a-1) is obtained, including the NHSE–SFL crossover. In addition, as in Fig. 2(b-1), the estimated critical length L_c (black dashed curve) agrees well with the value estimated from Fig. 2(a-1). As seen in Figs. S1(c-1,d-1), the regime diagram is not entirely symmetric with respect to $\mu = 1$; therefore, the values of κ_R for $\ln \mu = -0.5$ and $\ln \mu = 0.5$ are not identical.

For the same values of μ , Figs. S3(b,d) presents the entanglement phase diagram and the scaling laws for several values of λ , in a manner similar to Fig. S2. As with the low- μ case in Fig. S2, the phase diagram is consistent with that derived from the condition number in Figs. S3(a,c), respectively.

In summary, the introduced non-normality ratio introduced here can serve as a measure to construct regime diagrams, complementing the EE, as demonstrated in Fig. 2 in the main text and Fig. S3. We additionally remark that the non-normality ratio has a practical advantage, as it is much less numerically demanding compared to the EE, while still reliably distinguishing between the SFL, extended, and localized regimes.

V. DISCONNECTION OF AN IMPURITY BOND VIA QUASIPERIODICITY

In this section, we analyze how quasiperiodicity suppresses hoppings across the impurity bond and in the bulk. To verify that the quasiperiodicity decouples the impurity bond links prior to the bulk links, we examine the ratio of their expectation values defined as:

$$\frac{\left| \mu J \langle e^\alpha c_1^\dagger c_L + e^{-\alpha} c_L^\dagger c_1 \rangle \right|}{\left| J \langle e^\alpha c_{\text{bulk}}^\dagger c_{\text{bulk}+1} + e^{-\alpha} c_{\text{bulk}+1}^\dagger c_{\text{bulk}} \rangle \right|}. \quad (\text{S15})$$

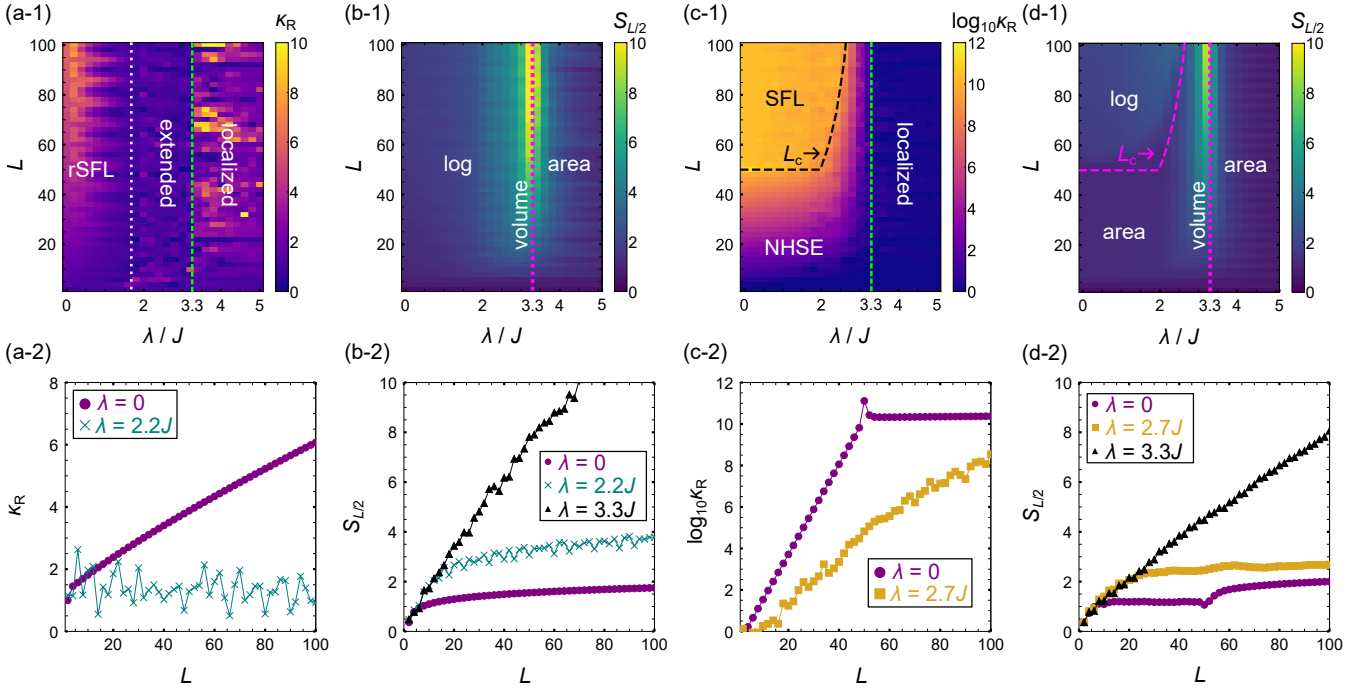


FIG. S3. (a,c) Non-normality ratio-based regime diagrams, (b,c) EE-based regime diagrams on the (λ, L) plane and (a-2,c-2) Scaling behavior of the non-normality ratio κ_R and (b-2,d-2) of the EE $S_{L/2}$ for (a,b) $\ln \mu = 0.5$ and (c,d) $\ln \mu = 25$. The dashed curve in (c-1,d-1) marks the critical length L_c estimated from Fig. 2(a-1) as in Fig. 2(b-1,c-1).

Here, we define the expectation value of the operator \hat{O} as

$$\langle\langle \hat{O} \rangle\rangle := \frac{1}{L} \sum_{n=1}^L \langle\langle E_n | \hat{O} | E_n \rangle\rangle, \quad (\text{S16})$$

where $|E_n\rangle$ ($|E_n\rangle\rangle$) denotes the n -th right (left) eigenstate. The calculated results are shown in Fig. S4. The behavior of this ratio confirms that the hopping across the impurity bond is effectively decoupled for $\lambda < \lambda_c$. The corresponding value of λ is consistent with the estimate ($\lambda \approx 2.6J$) obtained from Fig. 2(a-1) for $\alpha = 0.5$, $L = 89$ and $\ln \mu = -25$. For this parameter set, we have $\lambda_c \approx 3.3J$. This conclusion remains robust regardless of the choice of other bonds, provided they are located sufficiently deep within the bulk.

[1] C.-X. Guo, C.-H. Liu, X.-M. Zhao, Y. Liu, and S. Chen, *Phys. Rev. Lett.* **127**, 116801 (2021).
[2] Y.-C. Wang, H. H. Jen, and J.-S. You, *Phys. Rev. B* **108**, 085418 (2023).
[3] L. Li, C. H. Lee, and J. Gong, *Commun. Phys.* **4**, 42 (2021).
[4] Y. O. Nakai, N. Okuma, D. Nakamura, K. Shimomura, and M. Sato, *Phys. Rev. B* **109**, 144203 (2024).
[5] K. Kawabata, T. Numasawa, and S. Ryu, *Phys. Rev. X* **13**, 021007 (2023).
[6] L. Zhou, *Phys. Rev. B* **109**, 024204 (2024).
[7] S.-Z. Li, X.-J. Yu, and Z. Li, *Phys. Rev. B* **109**, 024306 (2024).

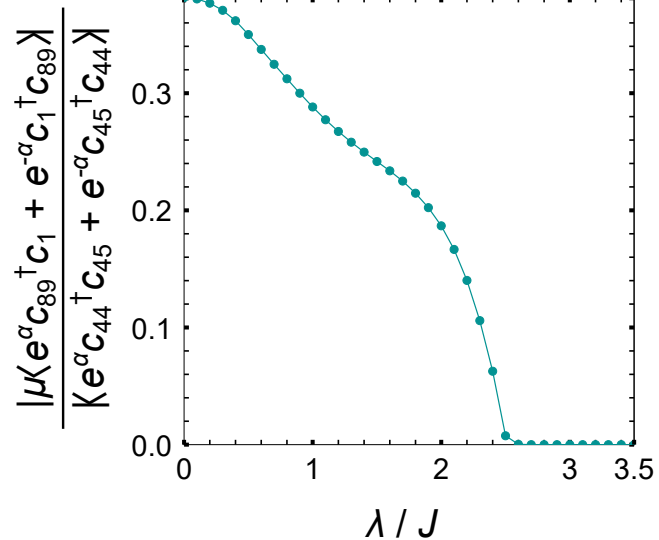


FIG. S4. Ratio of the absolute value of the boundary hopping expectation to that of the bulk hopping as a function of the quasiperiodic potential strength λ . The bulk hopping is evaluated between the $\lfloor L/2 \rfloor$ -th and $(\lfloor L/2 \rfloor + 1)$ -th sites. Here we adopt the same parameter set as in Fig. 3 in the main text, leading to $\lambda_c \approx 3.3J$.